Available online at www.sciencedirect.com

SciVerse ScienceDirect

Geochimica et Cosmochimica Acta 75 (2011) 6988–7005

Geochimica et Cosmochimica Acta

www.elsevier.com/locate/gca

Tree-mycorrhiza symbiosis accelerate mineral weathering: Evidences from nanometer-scale elemental fluxes at the hypha–mineral interface

Steeve Bonneville [a,*], Daniel J. Morgan [a], Achim Schmalenberger [c,1], Andrew Bray [a], Andrew Brown [b], Steven A. Banwart [c], Liane G. Benning [a]

[a] *Earth Surface Science Institute, School of Earth and Environment, University of Leeds, Leeds LS2 9JT, United Kingdom*

[b] *Leeds Electron Microscopy and Spectroscopy Centre, Institute for Materials Research, SPEME, University of Leeds, Leeds LS2 9JT, United Kingdom*

[c] *Kroto Research Institute, Department of Civil and Structural Engineering, University of Sheffield, Sheffield S3 7HQ, United Kingdom*

Received 27 April 2011; accepted in revised form 29 August 2011

Abstract

In soils, mycorrhiza (microscopic fungal hypha) living in symbiosis with plant roots are the biological interface by which plants obtain, from rocks and organic matter, the nutrients necessary for their growth and maintenance. Despite their central role in soils, the mechanism and kinetics of mineral alteration by mycorrhiza are poorly constrained quantitatively. Here, we report *in situ* quantification of weathering rates from a mineral substrate, (0 0 1) basal plane of biotite, by a surface-bound hypha of *Paxillus involutus*, grown in association with the root system of a Scots pine, *Pinus sylvestris*. Four thin-sections were extracted by focused ion beam (FIB) milling along a single hypha grown over the biotite surface. Depth-profile of Si, O, K, Mg, Fe and Al concentrations were performed at the hypha–biotite interface by scanning transmission electron microscopy-energy dispersive X-ray spectroscopy (STEM-EDX). Large removals of K (50–65%), Mg (55–75%), Fe (80–85%) and Al (75–85%) were observed in the topmost 40 nm of biotite underneath the hypha while Si and O are preserved throughout the depth-profile. A quantitative model of alteration at the hypha-scale was developed based on solid-state diffusion fluxes of elements into the hypha and the break-down/mineralogical re-arrangement of biotite. A strong acidification was also observed with hypha bound to the biotite surface reaching pH < 4.6. When consistently compared with the abiotic biotite dissolution, we conclude that the surface-bound mycorrhiza accelerate the biotite alteration kinetics between pH 3.5 and 5.8 to ~0.04 μmol biotite $m^{-2}h^{-1}$. Our current work reaffirms that fungal mineral alteration is a process that combines our previously documented bio-mechanical forcing with the μm-scale acidification mediated by surface-bound hypha and a subsequent chemical element removal due to the fungal action. As such, our study presents a first kinetic framework for mycorrhizal alteration at the hypha-scale under close-to-natural experimental conditions.

1. INTRODUCTION

Rock weathering of continental surfaces not only results in soil formation, upon which the whole of the biosphere depends, but also controls the long term chemical composition of groundwaters, rivers, lakes and oceans (Godderis et al., 2009). Over geological time, the weathering of rocks and, in particular of Mg- and Ca-silicates, exerts a major control on the level of atmospheric CO_2 and thus on

* Corresponding author. Present address: Unité de « Biogéochimie et Modelisation du Systeme Terre », Département des Sciences de la Terre (DSTE), Université Libre de Bruxelles (ULB), 50 Av. F. D. Roosevelt, B-1050 Brussels, Belgium. Tel.: +32 26502204.

E-mail address: steeve.bonneville@ulb.ac.be (S. Bonneville).

[1] Present address: Department of Life Sciences, University of Limerick, Schrodinger Building, Limerick, Ireland.

0016-7037/$ - see front matter © 2011 Elsevier Ltd. All rights reserved.
doi:10.1016/j.gca.2011.08.041

Earth's climate (Berner, 1995), through the formation of carbonate-rich minerals sequestering carbon. Of particular relevance, is the biological component of the mineral weathering. The evolutionary development of plants during the Phanerozoic coincides with large drops in atmospheric CO_2 levels (Crane et al., 1995; Kendrick and Crane, 1997; Berner and Kothavala, 2001; Berner, 2003). The concept underpinning these observations is that the emergence of plants with root systems on land increased terrestrial weathering significantly and enhanced carbon sequestration rates in marine system (Berner, 1992; Derry, 2006; Kennedy et al., 2006). This assertion has been strengthened by the work of Moulton et al. (2000). In two catchment basins of similar lithology and climate but differing in vegetation cover (tree-vegetated *vs.* bare or partially covered by lichens and mosses), trees accelerate four-folds the weathering rate release of Ca and Mg into streams. Other calculations from the same study indicate that plagioclase and pyroxene weather 2 and 10 faster respectively in the tree-covered catchment. Tree-roots and the way they interact with rocks in soil are crucial to the weathering enhancement.

However, roots are far from being bare of life. The rhizophere indeed host a large biomass and diversity of soil microorganisms (Kent and Triplett, 2002), in particular of fungi in symbiosis with roots. Mycorrhiza is the absorptive interface by which plants acquire nutrients (Landeweert et al., 2001). These mycorrhizal fungi forms vast networks of microscopic filaments (hypha – up to 1 mm long for 1–10 μm wide) that represent cumulative lengths of, on average, 100 km of filament per kg of soil with local upper limits of cumulative length reaching 600 km (Whitfield, 2007). Mycorrhiza receive an energy supply from their host plant equivalent to 20–30% of the carbon fixed during photosynthesis (Ek, 1997; Hobbie and Wallander, 2006). In return, they supply a large array of elements (i.e., Mg, Fe, etc) and nutrients (e.g., K and P) to the plant roots (Hogsberg and Hogsberg, 2002; Smits et al., 2008). Mycorrhiza are present at the global scale on Earth's surface: recent surveys found that 92% of present-day plant families, and 80% of all known plant species are mycorrhizal (Bonfante, 2003; Wang and Qiu, 2006). Given their ubiquitous character in soils, their vast biomass and thus their massive surface area available to interact with rocks, mycorrhiza are key agents of biotic rock weathering. Yet, the mechanisms and especially the kinetics of fungal weathering, are not well understood.

Mycorrhizal fungi can adopt various strategies to alter minerals and gain access to nutrients. A much-emphasized alteration pathway of mycorrhiza is the modification of key chemical parameters such as the pH and redox status of the soil solution (Gadd, 2007 and references therein). The production and excretion of low molecular weight organic compounds into soil solutions acting as ligands and/or siderophores that enhance the dissolution of minerals directly are well established (Adeyemi and Gadd, 2005; Ehrlich, 1998; Leyval et al., 1993). This purely "aqueous" viewpoint overlooks the fact that in most soils and also in experiments, the vast majority of soil microorganisms: bacteria (Bonneville et al., 2006; Buss et al., 2007; Amalfitano and Fazi, 2008; Tobler et al., 2008; Pote et al., 2010) and fungi (Gadd, 2007; Bonneville et al., 2009) strongly attach themselves to mineral surfaces. This attachment of microorganisms to soil particles is central to the physical coherence of soils and probably helps to form organic matter-mineral aggregates (Jastrow et al., 1998; Mikutta et al., 2009).

Fungal weathering of primary mineral has been mainly studied in pot experiments in symbiosis with plants/trees (Mojallali and Weed, 1978; Leyval and Berthelin, 1991; Wallander, 2000), in petri-dish mono-cultures (Paris et al., 1995) or in liquid mono-cultures (Lian et al., 2007; Balogh-Brunstad et al., 2008a). In all these studies, weathering resulted from multiple components of the experimental systems, e.g., water content, organic acid exudation and other metabolic/nutritional needs of the mono-culture or of the whole soil biota. Due to this combination of possible alteration pathways, it is difficult to quantify the relative contribution of fungi to the overall mineral weathering process.

In Bonneville et al. (2009) we used a tree–fungi–mineral continuum microcosm setup that permits sampling and measurements of the alteration directly at and below the interface between fungi and the mineral substrate (biotite), while excluding all other weathering contributions. Our experimental approach replicates (i) the fundamental biological relationship of the plant–fungi symbiotic systems in nature, (ii) hyphal phenotypes found in nature and (iii) the typical growth pattern encountered in soils (unsaturated water conditions). Using a combination of FIB ion milling to sample hypha–biotite ultrathin sections and high-resolution STEM-EDX to analyze the concentrations of K and Si, we demonstrated that a substantial removal of K and as well as a Fe(II) oxidation process (Bonneville, et al. 2009). Interestingly in concomitance with the chemical alteration, selected area electron diffraction (SAED) showed that a significant deformation of the biotite lattice structure occurs when hypha enter in contact with its mineral substrate (Bonneville et al., 2009). Therefore, the physical interaction between mycorrhizal hypha and mineral surfaces creates sub-μm-scale mechanical stresses in the near surface layers of the mineral structure (Bonneville et al., 2009). Potentially, these bio-mechanical stresses may evolve all the way to form channels (Balogh-Brunstad et al., 2008a) or tunnels penetrating the mineral (Jongmans et al., 1997). Although the contact zone between mycorrhiza (and by extension soil microorganisms) and minerals represents a small fraction of the total soil surface area (probably <1%, Young and Crawford, 2004), the unique capability of fungi to couple mechanical and chemical alteration processes makes the mineral–mycorrhiza interface the hotspot of the *weathering engine* at work in soils.

Here, our aims were (i) to measure the changes in elemental composition (Si, O, K, Mg, Fe and Al) at the fungi/mineral interface and into the substrate in four FIB sections sampled along a single biotite-bound hypha, (ii) to quantify the rate of alteration of surface-bound hypha and finally (iii) to develop a quantitative model of fungal weathering at the hypha scale. This article also compares consistently hyphal and abiotic biotite alteration kinetics in order to determine the efficiency of mycorrhiza to alter biotite in close-to-natural conditions. Thus, we measured

the pH of the micro-environment formed around hypha using pH-sensitive probe and determined as well the abiotic dissolution rates for the same biotite as used in the fungal experiments. All these data are then used to compare and discuss abiotic and mycorrhizal biotite weathering rates and kinetics and ultimately provide quantitative evidence that mycorrhiza bound to mineral surfaces and grown in symbiotic association with living tree/plant roots can accelerate mineral weathering.

2. MATERIALS AND METHODS

2.1. Plant-mycorrhiza symbiosis and incubation with biotite

Our experimental approach relied on growing the ectomycorrhizal fungi, *Paxillus involutus*, in symbiosis with *Pinus sylvestris* (Scots Pine). Seeds of *P. sylvestris* were surface-sterilized and then incubated aseptically in agar plates (see Bonneville et al., 2009 for composition). In parallel, *P. involutus* was grown in sterile square petri dishes on cellophane covering a modified Melin–Norkrans agar medium (see Bonneville et al., 2009 for composition). After a month of growth, both the Scots Pine seedlings and *P. involutus* cultures were transferred into a new petri dish, with the shoot of the tree protruding through a slot of the dish. After 10 weeks of common growth, the roots of the tree seedlings, now well-colonized by their fungal symbiont, were transferred into a final experimental microcosm consisting of a sterile square petri dish, containing 80 mL nutrient agar (Rorison medium – Bonneville et al., 2009) and 20 mL of Noble nutrient agar separated by a sterilized cellophane layer to prevent root and mycorrhiza penetration into the nutrient agar layer. This last transfer into the final microcosm insures that all hypha growing in the microcosm are mycorrhizal, i.e., grown in symbiosis with the root system of the Scots pine. Before solidification of the agar, HCl-washed and autoclaved perlite, inert amorphous volcanic glass, was sprinkled over the top agar layer. Finally, a previously autoclaved (20 min at 121 °C) biotite flake (Moen, Norway, ~0.5 × 1 cm) was cleaved and laid flat on the perlite grains (Fig. 1A). The tree–mycorrhiza–biotite microcosm system was then incubated for 130 days in a climate controlled room at 15 °C day and 10 °C night temperature, with an 18 h photoperiod at a photon flux of 550 μmol m^{-2} s^{-1} and with the shoots exposed to ~80% humidity. During this period, the biotite flake was colonized exclusively by mycorrhizal mycelium and did not experience any direct contact with the tree roots. The biotite flake was retrieved from the microcosm on the day of the ultra-thin section preparation for high-resolution micro-spectroscopic analysis.

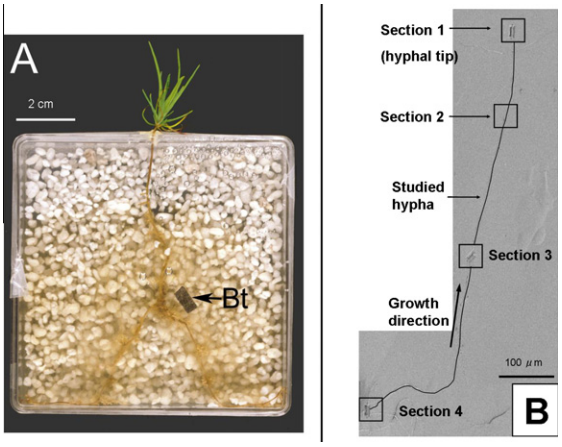

Fig. 1. (A) Experimental microcosm showing the location of the biotite flake colonized by *P. involutus* (Bt). (B) FEG-SEM micrograph of the sampled hypha on the (001) basal plane of the biotite flake studied with the location of the four FIB sections forming a sequence of increasing exposure time from section 1 to section 4.

2.2. Sampling and chemical analysis of hypha–biotite interface

Using a Focused Ion Beam (FIB – dual-beam FEI Nova 200 NanoLab), a relatively isolated but continuous hypha (~1000 μm) firmly attached to a biotite basal plane was sectioned at four locations at ~2, 135, 400 and 740 μm (sections 1 to 4, respectively) away from the hypha tip (Fig. 1B). Full details of the FIB-sectioning protocols can be found in Bonneville et al. (2009). The hypha–biotite FIB sections were analyzed using a Philips/FEI CM 200 Field Emission Gun (FEG) transmission or scanning transmission electron microscope (TEM/STEM) operated at 197 kV and equipped with an ultra-thin-window Energy Dispersive X-ray detector (EDX, Oxford Instruments) and a Gatan Imaging Filter (GIF200). A double-tilt sample holder was used to orient the FIB sections such that the TEM viewing direction was normal to the biotite–hypha interface. Elemental X-ray intensity profiles (EDX line-scans) of between 400 and 1000 nm in length across each interface were recorded in STEM mode with a minimum electron beam diameter of 5 nm. The line-scans were recorded at a 1.5–3.9 nm step size along a line perpendicular to the biotite–hypha interface in the [001] direction, normal to the (001) cleavage plane (see Bonneville et al., 2009 – Repository Data Fig. DR3). The intensities in counts s^{-1} of the Kα X-ray lines of Si, Al, Mg, Fe, O and K were recorded as a function of probe position sequentially (dwell time of a few msec for each probe position) and multiple time over the acquisition time of the profile (~10 min). We have shown before (Bonneville et al., 2009) that irradiation damage to the reacted biotite was negligible for the first 30 min of continuous exposure using the STEM-EDX settings described above. Finally, the bulk chemical composition of the freshly cleaved biotite was determined by Electron Microprobe Analysis (EMPA – Cameca SX50 equipped with three wavelength detectors and an Oxford Instruments INCA 250 EDX system) operated at 15 kV and 15 nA. The general EMPA-derived formula for our biotite from an average of 25 spot measurements was $K_{0.917}$ $Na_{0.018}$ (interlayer) $Mg_{0.763}$ $Mn_{0.055}$ $Fe_{1.612}$ $Cr_{0.002}$ $Al_{0.227}$ $Ti_{0.194}$ (octahedral sheet) $Al_{1.263}$ $Si_{2.737}$ (tetrahedral sheet) $(OH)_2$ O_{10}). This pristine biotite composition was used as a reference chemical composition to determine the

compositional changes across the hypha–biotite interface from the STEM-EDX line-scans.

2.3. Hyphal pH measurements

The pH around living hypha growing in the microcosm experiments were measured by Confocal Laser Scanning Microscopy (CLSM) with an inverted Zeiss microscope with a Meta510 detector (Zeiss, Jena, Germany) and an argon multiphoton laser at 488 nm. The molecular probe SNARF4F (Invitrogen, Paisley, UK) was used at 5 μM concentration to determine the pH of the hyphal microenvironments. This molecular probe possesses two specific characteristic fluorescence emission bands at 580 and 640 nm respectively for its acidic and basic forms. By ratioing the fluorescence at the two wavelengths, this method becomes independent of the dye concentration, photobleaching, and changes of instrumental conditions such as optical path length, excitation intensity, or detector sensitivity (Marcotte and Brouwer, 2005). A pH-calibration (Fig. S1) using micro-slide wells (Ibidi, Martinsried, Germany) was done by adding 5 μM of SNARF4F to 0.2 mL of a 50 mM phosphate buffer at pH 4.6, 5.0, 5.4, 5.8, 6.2, 6.6, 7.0, 7.4, 7.8 and by calculating the mean value in a histogram of the 547–587 and 619–661 nm channels (Photo-Paint 13, Corel, Ottawa, Canada) (Hunter and Beveridge, 2005). Ratios of fluorescence emitted at those two wavelengths recorded at the different pH values were then fitted with a Boltzmann sigmoid fit (Fig. S1). After calibration, reacted biotite flakes from two parallel microcosms systems colonized by *P. involutus* and containing both biotite-surface attached as well as aerial (i.e., non attached) hyphae in close vicinity to the plant roots but off the biotite were imaged and analyzed. Approximately 50 μL of a 5 μM SNARF4F solution was delivered directly onto the colonized biotite flake or on aerial fungal hypha immediately after being removed from the microcosm system. A cover slip was placed on top of the biotite flake or the aerial hypha. The samples were "sandwiched" between cover slip and glass slide and the open sides were sealed with varnish. Confocal microscopy analysis started after 15 min of incubation at room temperature in the dark. Pixel ratios of selected areas of interest of the CLSM images were calculated and the pH determined using the calibration curve (Fig. S1). The standard deviation error of our pH-probe method is ~0.1 pH unit above pH 5.5 but increased to 0.35 pH units for pH below 5.5. Typical CLSM images have a pixel size of 0.14 × 0.14 μm by 0.5 μm in focal depth and the hyphal pH measurements areas are ~2 × 5 μm.

2.4. Abiotic dissolution of biotite

Biotite, from the same source as used in the fungal microcosms, was powdered and sieved to obtain the 75–150 μm size fraction. Fine particles were removed by repeated sonication and gravitational settling and the powder subsequently dried. The specific surface area for the biotite powder ($2.63 \pm 0.08\ m^2\ g^{-1}$) was determined by N_2-BET (Micromeritics Gemini V analyzer). The cleaned biotite was imaged with a Field Emission Gun Scanning Electron Microscope (FEG-SEM, Leo/Zeiss Gemini 1530) operated at 3 kV with sample coated with 3 nm of platinum. FEG-SEM images were recorded on a 45° angle with respect to the incident electron beam tilted samples holder. The basal and edge dimensions of ~20 representative individual particles were measured to determine the average dimensions of the biotite particles and to define the relative contribution of basal (SA_{basal}) and edge (SA_{edge}) planes to the total surface area (SA_{total}) of the particles.

Abiotic dissolution experiments were carried out in batch and in flow-through mode, both at an ionic strength of 0.01 m and at pH 2 and 4 (batch) and 3.3 (flow-through). The ionic strength was fixed using $CaCl_2$ (concentration of 0.0033 M) and the pH adjusted using HCl. For the batch dissolution experiments, 0.5 g of biotite was reacted for 12 h with 500 mL of a 0.01 m $CaCl_2$ solution at 25 °C under constant shaking at 140 rpm. Over this period, 20 aliquots of 1 mL each of the suspension were collected and filtered through 0.2 μm filters directly into dilute 3% HNO_3. The aqueous concentrations of Mg, Fe and Al were analyzed by Inductively Coupled Plasma-Mass Spectrometry (ICP-MS, Perkin Elmer Elan DRC II). Ranges of Relative Standard Deviation (RSD) across the set of sample analyzed were for Al: 0.21–5.53%; Mg: 0.21–3.74%; Fe: 0.29–5.81%.

Three flow-through biotite dissolution experiments were carried out in a 300 mL titanium Parr™ mixed-flow reactor with controlled temperature, pressure and stirring as well as continuous pH monitoring (Wolff-Boenisch et al., 2004). In brief, between 3 and 6 g of biotite powder was placed into the stirred at ~400 rpm in a reactor with 0.01 M $CaCl_2$ solution at 25 °C and pH 3.3 (the pH did not vary more than 0.1 pH units). The flow through system was operated continuously for 80 h by pumping 0.01 M $CaCl_2$ solution through the reactor using a high-performance liquid chromatography (HPLC) pump at flow rates ranging from 0.07 to 0.13 L h^{-1} depending on the experiment. At the system outlet, the liquid passing through a 2 μm titanium filter was collected regularly directly into pre-acid-cleaned plastic bottles that were pre-acidified with dilute 0.5 % HNO_3. In the flow-through experiments, only the total dissolved Si concentration was analyzed as a proxy for biotite dissolution using by a colorimetric method (Fishman and Friedman, 1989) and a Varian Cary 50 Bio UV-Visible spectrophotometer at 700 nm.

3. RESULTS

3.1. Hyphae–biotite interfaces in the STEM elemental profiles

Fig. 1B shows that the hypha sampled by the FIB sectioning, grew over a smooth (0 0 1) basal plane biotite surface. Even at higher resolution, the hypha–biotite interface is extremely well-defined and atomically sharp. In no cases were localized penetrations or etch-pits visible at the biotite–hyphae contact zone (see Fig. 2 in Bonneville et al., 2009). Four STEM elemental line-scans were acquired perpendicularly to the hypha–biotite interface across each FIB section (one example of a STEM dataset for Si, O and K for section 4 is shown in Fig. 2A). In biotite, Si is the

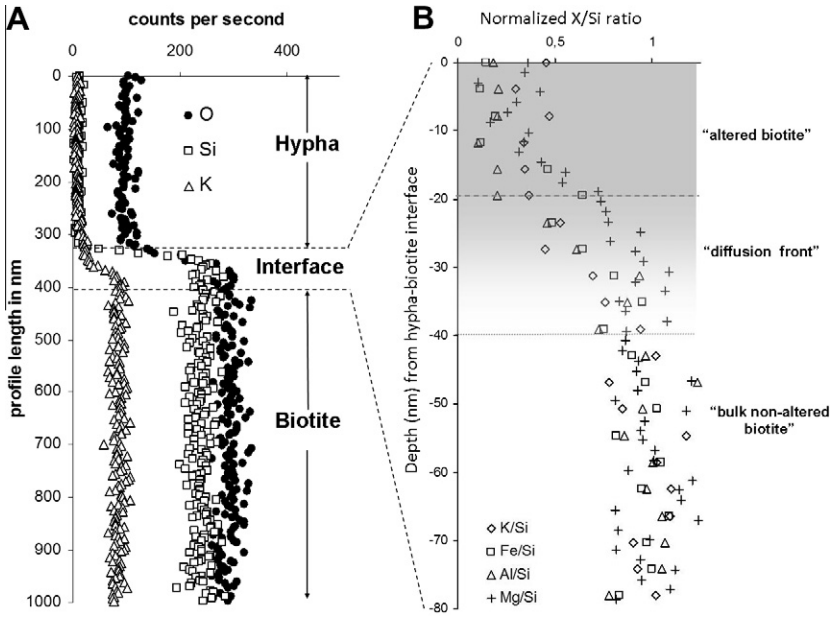

Fig. 2. (A) STEM-EDX line-scan profiles of Si, O and K across the hypha–biotite interface for FIB-section 4; note that Si and O exhibit similar profiles and the hypha–biotite interface position was set using the median Si counts (Eq. (1)) as shown in Supplementary Fig. S2. (B) K, Fe, Al and Mg ratios to Si in the topmost 80 nm of biotite directly underneath the hypha in FIB-sections 4 (results for section 1 to 3 are shown in Fig. S4). Note that all elemental ratios have been normalized between 0 and 1 with respect to the average bulk, non-altered, biotite ratio far below the interface in each FIB section (see text in Section 3.2). The gray zones above the dashed lines in Fig. 2B and S4 indicate the "altered biotite" layer, while the gray shaded zone between the dashed and dotted lines represent the "diffusive front" zone in sections 3 and 4 and below the dotted line is the "bulk non-altered biotite". Standard deviations (in percent) for normalized K/Si, Fe/Si, Al/Si and Mg/Si ratio were 15%, 13%, 15% and 17%, respectively.

main element and the change in Si peak intensity in the STEM line-scans (in counts s^{-1}) served as a proxy to position the physical interface between the biotite and the hypha. This is exemplified in Fig. S2 where a sharp transition in the Si profile between ~320 and 345 nm is clearly visible. Within this 25 nm zone, the Si peak intensity quickly increased from an average background level of $\sim 12 \pm 4$ counts s^{-1} ($\overline{Si_H}$) before the biotite edge, to 239 ± 17 counts s^{-1} ($\overline{Si_{Bt}}$) on average in the biotite. From such data, the median Si counts (Si_{Med}) was calculated as follows:

$$Si_{Med} = \frac{(\overline{Si_{Bt}} - \overline{Si_H})}{2} + \overline{Si_H} \quad (1)$$

Subsequently, we placed the physical interface between the hypha and the biotite at the Si_{Med} intensity value in the Si profile (for FIB section 4 illustrated in Fig. S2 the Si_{Med} is at 336 nm). The above procedure for Si was used to position the physical interface within each of the four FIB sections because there was no evidence of Si loss from the biotite during hyphal contact (Bonneville et al., 2009). The Si-defined interface (Si_{Med}) was then taken to be the origin of the biotite elemental profiles in all the FIB sections (i.e., from here on, 0 nm depth = physical fungal–mineral interface). This method also allowed us to determine the experimental thickness/sharpness of the chemical interfaces between the hypha and the biotite. Of the elemental profiles measured across the biotite–hypha interface in each section, we selected the datasets with the sharpest interface (shortest Si interface, ~25 nm, Fig. S2 for FIB section 4).

3.2. Chemical composition of the biotite–hypha interface

After positioning the hypha–biotite interface in each line-scan profile, the peak intensities for K, Al, Mg and Fe measured in each FIB section were ratioed to Si at any given depth. Away from the interface with the hypha, that is, in the bulk non-altered biotite (e.g., from 450 to 1000 nm in the profile in Fig. 2A), the average peak intensities for K, Al, Mg and Fe normalized to Si were very consistent from FIB section to FIB section (Fig. S3 and figure caption for standard deviations). These results demonstrate that: (i) the chemical composition of the bulk non-altered biotite is essentially constant in all four FIB sections (hypha grow over a homogenous mineral substrate); and (ii) the STEM-EDX elemental profiles can therefore be used to give a robust quantification of the concentrations of elements in the different FIB sections and also within a single FIB section as a function of depth. For practical reasons, K/Si, Fe/Si, Al/Si and Mg/Si intensity ratios in each of the sections were normalized as described here for potassium:

$$(K/Si)_{no} = \frac{(K/Si)}{(K/Si)_{Bt}} \quad (2)$$

where $(K/Si)_{Bt}$ is the average intensity ratio of K relative to Si measured in the bulk non-altered biotite and (K/Si) is the intensity ratio measured at any given depth. In doing so, the normalized intensity ratio, $(K/Si)_{no}$ will vary with depth from a value of 0 (i.e., complete depletion) to 1 (i.e., pristine biotite).By normalizing the whole depth pro-

Table 1
Release rates and standard deviations for Mg, Fe and Al from the abiotic biotite batch dissolution experiments at pH 2, 4 and the flow through experiments at pH 3.3 at 25 °C and corresponding biotite alteration rates calculated from the molar fraction of the elements in the biotite formula as determined with EMPA (Bonneville et al., 2009).

Abiotic bulk biotite dissolution ($\times 10^{-6}$ mol element m^{-2} h^{-1})	Mg	Fe	Al	Si
Batch: pH 2 release rate of elements	1.29 ± 0.13	1.52 ± 0.12	1.50 ± 0.13	–
Batch: pH 4 release rate of elements	0.17 ± 0.04	0.20 ± 0.06	0.08 ± 0.03	–
Batch: pH 2 – biotite dissolution rate (r_{bulk})[a]	1.7 ± 0.14	0.94 ± 0.07	1.0 ± 0.08	–
Batch: pH 4 – biotite dissolution rate (r_{bulk})[a]	0.22 ± 0.05	0.14 ± 0.03	0.05 ± 0.02	–
Flow-through steady state dissolution rate at pH 3.3 (r_{bulk})[a]	–	–	–	0.18 ± 0.01

[a] Using biotite formula: $K_{0.917}$ $Na_{0.018}$ $Mg_{0.763}$ $Mn_{0.055}$ $Fe_{1.612}$ $Cr_{0.002}$ $Al_{1.49}$ $Ti_{0.194}$ $Si_{2.737}$ $(OH)_2$ O_{10}.

file to the average chemical composition of the bulk biotite, the progressive removal of elements from the biotite at the interface with the hypha within each FIB section becomes clearly visible with increasing distance from the tip (i.e., from FIB section 1 to FIB section 4 in Fig. 2B and S4; note that for clarity only the first 80 nm below the interface were plotted). In FIB sections 1 and 2 (Fig. S4), the normalized intensity ratios were unchanged for Mg, Al and Fe from the interface all the way into the bulk biotite with ratios all ~1. Only K showed a slight depletion, $(K/Si)_{no}$ down to 0.27, in the first 5–7.5 nm from the interface in section 1 and a slightly clearer removal trend in section 2, where $(K/Si)_{no}$ is as low as 0.5 within the first 10 nm from the hypha–biotite interface. By contrast, sections 3 and 4 show significant depletions in all elements relative to the bulk biotite composition with $(K/Si)_{no}$, $(Mg/Si)_{no}$, $(Fe/Si)_{no}$ and $(Al/Si)_{no}$ ratios dropping respectively to minima of 0.02, 0.15, 0.04 and 0.1 at depths from the interface ranging from −15 to −20 nm depending on the FIB section and the element (dashed lines in FIB section 3 and 4 in Figs. S4 and 2B respectively). At greater depth (>20 nm), all normalized ratios progressively increase to reach values close to 1 at a depth of −35 to −40 nm from the interface depending on the element (dotted lines in FIB sections 3 and 4 in Figs. S4 and 2B). Overall, the profiles for sections 3 and 4 are indicative of a strong elemental removal from the top section of the biotite (topmost 40 nm) in contact with the hypha.

Within the two depth-profiles from FIB section 3 and 4, we can clearly distinguish three zones: (i) the top 15–20 nm where all normalized ratios are relatively constant at a minimal values (from here on referred to as "altered biotite", gray zone above the dashed lines in Figs. 2B and S4); (ii) between ~15–20 nm and up to ~40 nm a transient, curved trend of increasing normalized ratio with depth ('diffusive front', gray shadings between the dashed and dotted lines in Figs. 2B and S4); and (iii) the 'bulk non-altered' biotite in the deeper part of the profile (Figs. 2B and S4). Using these four datasets we quantified the elemental fluxes across the hypha–biotite interface as well as the mycorrhizal alteration rates, and developed an empirical model to describe our depth-profile data.

3.3. Abiotic dissolution of biotite

Abiotic dissolution experiments using the exact same biotite were carried out, to provide abiotic elemental release rates to compare with the mycorrhizal alteration experiments. The average SA_{basal}/SA_{total} and SA_{edge}/SA_{total} ratios of individual biotite particles as measured from the FEG-SEM micrographs were 0.94 and 0.06 (± 0.046, $n = 20$), respectively. For all batch systems, the initial 1.5 h of the experiments were characterized by fast elemental release that we ascribed to minor amounts of remnant fine biotite particles undergoing dissolution (see Fig. S5 for examples for the batch experiments at pH 2 and 4). After 1.5 h, the aqueous concentration of Mg, Fe and Al increased linearly with time over the course of the experiments. Linear regressions of the biotite dissolution data between 1.5 and 12 h allowed us to calculate the abiotic release rates for Mg, Fe and Al in mol m^{-2} h^{-1} and also to derive the abiotic biotite dissolution rates at pH 2 and 4 (Table 1) assuming the chemical formula measured by EMPA (see Section 2.2). For the flow-through experiments at pH 3.3 (Fig. S5), the first 45 h showed fast biotite dissolution rates (based on the Si concentrations and chemical formula) that progressively slow down and reached a steady-state dissolution rate at around 50 h. All abiotic elemental release and biotite dissolution rate values are listed in Table 1.

3.4. pH of the hypha microenvironment

pH measurements of the micro-environments around 8 living hypha growing either in intimate contact with the biotite surface or were near the root of the Pine tree and thus not in contact with the biotite, revealed a clear acidification when fungi were in contact with the biotite. Out of 32 measurement areas on biotite-bound hypha, 23 areas appeared to be below the detection limit of our method which was pH < 4.6 (Fig. 3A, and pH-calibration curve in Fig. S1), but 9 areas had pH values between 5.3 and 5.8 (Fig. 3C). For hypha not in contact with the biotite, out of 21 measurement areas, only 2 had a pH below 6 (Fig. 3B), while in all other areas, the pH ranged from 6.1 to 6.8 with on average of ~6.3 (Fig. 3D).

4. MODEL OF THE CHEMICAL WEATHERING AT THE HYPHA–BIOTITE INTERFACE

We have developed an empirical model describing the chemical changes measured in the biotite directly underneath the fungal hypha. The model is based on the concept of a moving weathering front within the biotite, leading to the development of a progressively deepening alteration

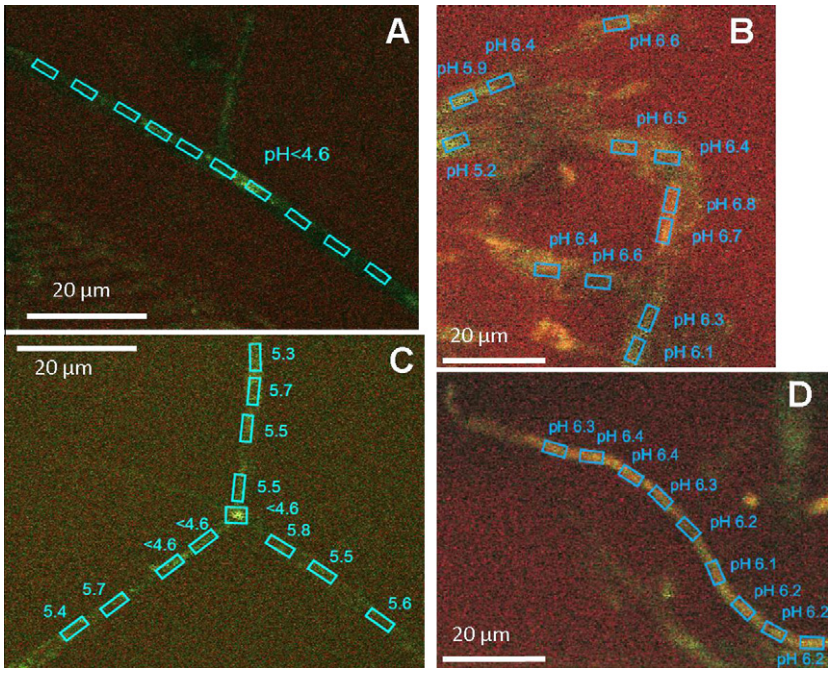

Fig. 3. CLSM images of surface-bound hypha in (A) and (C) and "aerial, near to the root" non biotite-bound hypha in (B) and (D) with their respective pH values as derived from the 580/640 nm fluorescence ratio. All values in (A) were <4.6.

layer with increasing time (Fig. 4). The four STEM profiles (Figs. 2B and S4) revealed that the hypha, strongly bound to the mineral surface, were able to impose and maintain a large chemical gradient inducing the diffusion of elements out of the biotite and into the hypha. The loss of major constitutive elements from the biotite destabilizes its lattice structure and leads to a mineralogical rearrangement into a metastable, secondary or "altered biotite" (Fig. 4). As

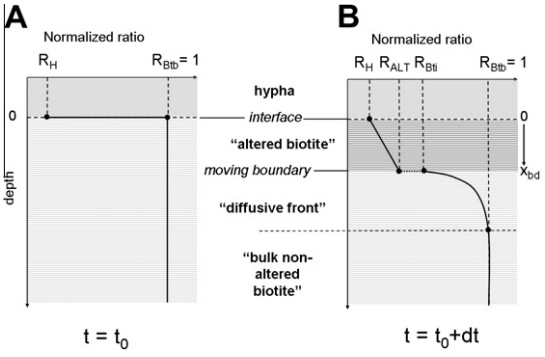

Fig. 4. Conceptual model for the alteration at the hypha–biotite interface. (A) Initial chemical profile (i.e., pristine biotite at the beginning of the colonization by the hypha; $t = t_0$;), (B) profile after exposure to living hypha ($t = t_0 + dt$). As alteration proceeds via solid-state diffusion, the chemical profile develops into three zones: the topmost part of the profile where, due to heavy depletion of cations, the biotite is transformed into "*altered biotite*"; which is separated from *the* "*diffusive front*" by a moving boundary which migrates progressively deeper into the "*bulk non-altered biotite*" zone.

the alteration and mineral transformation proceed within the biotite, the mobilized elements diffuse though a progressively thickening layer of "altered biotite". Thus, the thickness, the carrying capacity and the diffusive properties of the "altered biotite" directly influence the overall rates of diffusion and biotite breakdown. The model presented here assumes that, during contact, the physical mineral–hypha "interface" is immobile (i.e., a biotite solid-state transformation into a secondary phase takes place without dissolution of the Si–O structure (Bonneville et al., 2009)). This assumption is supported by our high resolution imaging and analyses of the hypha–biotite interface which showed *no* hypha penetration, or depressions, etch pits or volumetric changes of the mineral underneath the hypha, yet revealed the development of vermiculite-type mineral domains in the close vicinity (upper 30–50 nm) of the interface (Bonneville et al., 2009).

This moving boundary problem is analogous to the situation where ice is growing on top of an un-stirred water body or the development of an oxidized layer (tarnish) at the surface of elemental silver (Bennett et al., 1969; Crank, 1987). In our case, the moving boundary is located between the "diffusive front" in the biotite and the "altered biotite" layer, which migrates with time deeper into the biotite as mineral breakdown proceeds (Fig. 4). Our model also assumes mass conservation, i.e., the influx of elements into the "altered biotite" layer from the "diffusive front" is equivalent to the flux out of the "altered biotite" layer into the hypha. Furthermore, the "altered biotite" layer has fixed boundary conditions: (i) at the hypha–mineral interface, the chemical composition of the hypha is assumed to be constant (i.e., no elemental accumulation in the hypha

directly above the biotite, the elements removed are instead transferred by the hypha to the host–plant); and (ii) at the moving boundary (Fig. 4), the breakdown of the biotite into "altered biotite" occurs when the normalized elemental ratios drop below a fixed threshold that reflects a biotite stability limit. Since the "altered biotite" grows effectively from a zero thickness with constant boundary conditions, diffusion equilibria are established within the "altered biotite". Thus the normalized ratios in this "altered biotite" layer follow a linear gradient with depth (Fig. 4B; i.e., bold striped zone). Within this layer, at any depth, x_i (in m), the normalized ratio to Si of an element i, R_i, is:

$$R_i = \left(\frac{R_{ALT} - R_H}{x_{bd}}\right) x_i + R_H \quad (3)$$

where R_H is the normalized ratio of the element i at the physical interface between hypha and the mineral surface, and R_{ALT} is the normalized ratio of element i at the moving boundary between the "altered biotite" and the "diffusive front" in the biotite". The depth at which this moving boundary is positioned is defined as x_{bd}. These three parameters (R_H, R_{ALT} and x_{bd}) were determined for each section and each element (Table 2) by fitting the final model to the STEM-EDX elemental concentration profiles. Once determined, these parameters can also be used to calculate the flux of a given element, J_{ALT}, through the "altered biotite" layer into the hypha:

$$J_{ALT} = -D_{ALT} \frac{R_{ALT} - R_H}{x_{bd}} \quad (4)$$

where D_{ALT} is the diffusion coefficient of the element i in the "altered biotite" in $m^2\ s^{-1}$ (Table 2). Due to differential element partitioning between the "altered biotite" layer and the biotite in the "diffusive front", the model allows for a compositional discontinuity at the moving boundary (Fig. 4), as follows:

$$R_{ALT} = R_{Bti} \times K_P \quad (5)$$

With R_{Bti} being the value of the normalized ratio of element i, at which the biotite breaks down into "altered biotite" and K_P, the partition coefficient of i between "altered biotite" and the biotite affected by the "diffusive front" (both parameters determined from the fitting of the model to the STEM-EDX elemental concentration profiles; Table 2). The K_P term is necessary, as elemental diffusion must be continuous in terms of chemical potential across the moving boundary; the elemental abundance however is not necessarily continuous (and indeed, is not in this case). Within the biotite affected by the "diffusive front", the normalized ratios as a function of depth vary between R_{Bti} and 1 (the breakdown composition and the pristine biotite composition, respectively) and this is modelled as a one-dimensional error function distribution:

$$R_i = R_{Bti} + (1 - R_{Bti}) erf\left(\frac{x_i}{2\sqrt{D_{Bt} t_f}}\right) \quad (6)$$

from which, the flux of element i out of the biotite, J_{Bt}, through the moving boundary (from the "diffusive front" into the "altered biotite" layer) can be derived as:

$$J_{Bt} = D_{Bt} \frac{(1 - R_{Bti})\, erf\left(\frac{x_i}{2\sqrt{D_{Bt} t_f}}\right)}{\partial x_i} \quad (7)$$

where D_{Bt} is the diffusion coefficient of element i in the biotite in $m^2\ s^{-1}$, R_i the normalized element i ratio at depth x_i and t_f is the *fictive* time elapsed to reach the value on the profile for the element i. D_{Bt} was fixed to $3.8 \times 10^{-23}\ m^2\ s^{-1}$ for K in biotite (Taylor et al., 2000).

In the model, the ratio of diffusion coefficients D_{Bt} and D_{ALT} governs the curvature of the "diffusive front". Therefore, by fixing D_{Bt} and fitting the modelled curves to the depth profile data for K, an estimation of D_{ALT} but also the active time period of the alteration, t_r (see definition below) could be derived. In effect, K depth-profiles were used to time-calibrate the model (see Section 5.3 below). Classically in diffusion, the flux of any given element is proportional to the inverse of the distance of diffusion (Crank, 1987) and therefore, in our case, the flux, J_{ALT}, is proportional to $1/x_{bd}$ (Eq. (4)). The depth or distance of the diffusion is itself proportional to the square root of time, which means that J_{ALT} (Eq. (4)) and J_{Bt} (Eq. (7)) are dependant upon the inverse of the square root of the elapsed time t. As shown in Fig. S6, the latter relationship can be used to derive the *fictive* time, t_f from:

$$\frac{J_{Bt}}{J_{ALT}} = C^{St} \frac{\sqrt{t_f}}{\sqrt{t_1}} \quad (8)$$

where t_1 is a time fixed to 1 second and representing the time just after the hypha start interacting with the biotite and C^{st} is a constant. Thus, Eq. (8) can be rearranged into:

$$t_f = C^{St} \left(\frac{J_{Bt}}{J_{ALT}}\right)^2 \quad (9)$$

Even though t_f calculated via Eq. (9) yields the correct depth profile in the "diffusive front" – i.e., a good agreement between the modelled value and the normalized ratio for element i, it is, however, a *fictive elapsed time*. Indeed, as the "altered biotite" layer thickens, the concentration curve in the "diffusive front" is continuously "compressed" by the downward movement of the moving boundary (Fig. 4). Therefore, the derivation of the period of contact between hypha and biotite (for each FIB section) only based on the fitting of the concentration curve in the "diffusive front" would be erroneous (in fact, an underestimation) as it should also take into account the time required to form the "altered biotite" layer. The period of contact between hypha and biotite however can be estimated by introducing a "compression factor" of the diffusion front calculated as:

$$Q = \frac{\text{Total removal of element } i}{\text{Removal of element } i \text{ below boundary}} \quad (10)$$

with Q, being the ratio between the total amount removed of the element i (i.e., integrated throughout the entire depth profile) and the element removal calculated below the moving boundary (i.e., only in the 'diffusive front' part and for t_f). Q is then used to derive the actual time period (t_r in seconds, determined as discussed above and listed in Table 2) required to reach the depth-profile shape via:

$$t_r = t_f Q \quad (11)$$

Table 2
Parameters used for the modelling of the Fe, Al, K and Mg concentrations in the four FIB sections. R_{Bti}, R_H, R_{ALT}, K_P and x_{bd} were obtained by fitting to the experimental data (Fig. 5). D_{Bt} for the K profile was taken from Taylor et al. (2000) and D_{ALT} and t_r were outputs from the model. Note that the same D_{Bt}, D_{ALT}, R_{Bti}, R_{ALT}, R_H (except for K in section 2) and the K_P values were used consistently to fit each elemental profile across the four FIB sections.

FIB Sect.	R_{Bti} (ratio/mol μm^{-3})	R_H (ratio/mol μm^{-3})	R_{ALT} (ratio/mol μm^{-3})	K_P (–)	D_{Bt} (m^2 s^{-1})	D_{ALT} (m^2 s^{-1})	x_{Bd} (m)	t_r[a] (days)
Potassium								
1	0.63 3.8×10^{-15}	0.35 2.3×10^{-15}	0.5 3.0×10^{-15}	0.8	3.8×10^{-23}	3.1×10^{-22}	2.5×10^{-9}	0.41
2	0.63 3.8×10^{-15}	0.49 2.9×10^{-15}	0.5 3.0×10^{-15}	0.8	3.8×10^{-23}	3.1×10^{-22}	2.8×10^{-9}	13.5
3	0.63 3.8×10^{-15}	0.35 2.3×10^{-15}	0.5 3.0×10^{-15}	0.8	3.8×10^{-23}	3.1×10^{-22}	28×10^{-9}	61.4
4	0.63 3.8×10^{-15}	0.35 2.3×10^{-15}	0.5 3.0×10^{-15}	0.8	3.8×10^{-23}	3.1×10^{-22}	30.5×10^{-9}	72.8
Aluminium								
1	–	–		–	–	–	–	–
2	–	–		–	–	–	–	–
3	0.49 4.8×10^{-15}	0.15 1.5×10^{-15}	0.24 2.4×10^{-15}	0.49	4.4×10^{-23}	4.4×10^{-22}	18×10^{-9}	61.4 (48)
4	0.49 4.8×10^{-15}	0.15 1.5×10^{-15}	0.24 2.4×10^{-15}	0.49	4.4×10^{-23}	4.4×10^{-22}	21×10^{-9}	72.8 (61)
Magnesium								
1	–	–		–	–	–	–	–
2	–	–		–	–	–	–	–
3	0.6 3.0×10^{-15}	0.25 1.2×10^{-15}	0.45 2.25×10^{-15}	0.75	2.6×10^{-23}	1.3×10^{-22}	17×10^{-9}	61.4 (48)
4	0.6 3.0×10^{-15}	0.25 1.2×10^{-15}	0.45 2.25×10^{-15}	0.75	2.6×10^{-23}	1.3×10^{-22}	18.5×10^{-9}	72.8 (61)
Iron								
1	–	–		–	–	–	–	–
2	–	–		–	–	–	–	–
3	0.4 4.2×10^{-15}	0.15 1.6×10^{-15}	0.2 2.1×10^{-15}	0.5	5.6×10^{-23}	6.0×10^{-22}	14.5×10^{-9}	61.4 (48)
4	0.4 4.2×10^{-15}	0.15 1.6×10^{-15}	0.2 2.1×10^{-15}	0.5	5.6×10^{-23}	6.0×10^{-22}	15.5×10^{-9}	72.8 (61)

[a] The exposure period, t_r, was derived from the K/Si depth profiles (see Section 4 for details). Note that the effective, t_r, for Al, Fe and Mg are shorter because the diffusion of these elements started only after section 2; the actual diffusion periods – in days) for these elements are indicated in brackets.

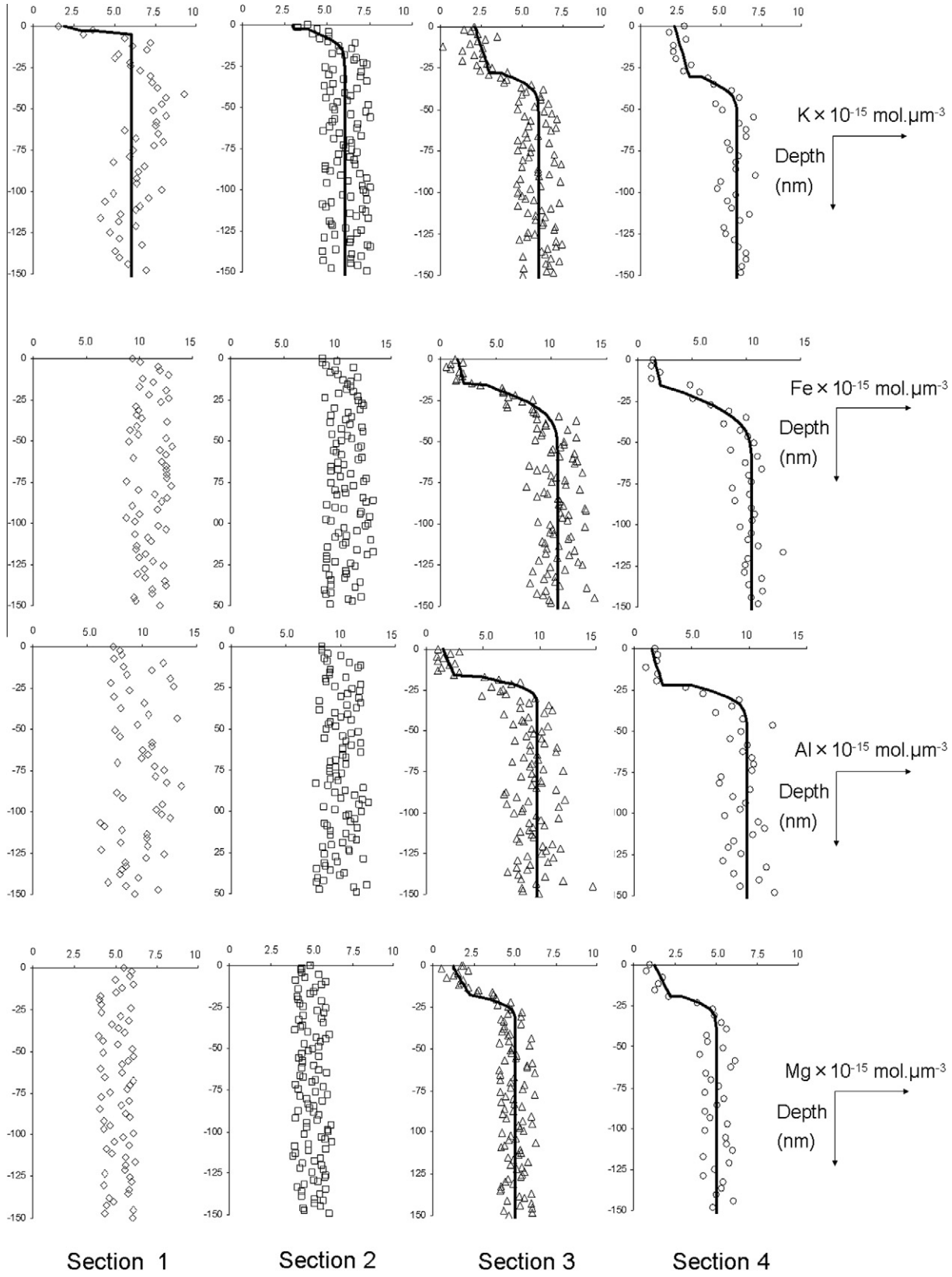

Fig. 5. Chemical (symbols) and modelled (lines) concentration depth-profiles over the 150 nm below the hyphae–biotite interface for K, Al, Fe and Mg in the four FIB sections. Note that only K is mobilized in all four sections in contrast to Al, Fe and Mg, which are only mobilized from the biotite in sections 3 and 4.

So far, the depth profile datasets and the outputs of our model were expressed in units of normalized ratios, varying between 0 and 1. However, to quantify the flux of elements out of the biotite, it is necessary to calculate from the normalized ratios, the concentration C_i (in mol μm^{-3}) of element i using:

$$C_i = \frac{R_i(\%wt_i)\rho}{Mm_i} \quad (12)$$

where R_i is the normalized ratio of element i (ranging between 0 and 1) at any given depth of the profile, $\%\ wt_i$ is the weight percent of element i in the bulk biotite (as quantified by EMPA), ρ the density of biotite (i.e., 3.08 g cm^{-3}) and Mm_i is the molar mass of element i. The fits of the above model to the profiles of the elemental concentration per unit volume (converted from the as-measured STEM-EDX intensity profiles using Eq. (12)) are plotted for each FIB section for Al, Mg, K and Fe in Fig. 5. The quality of the fits is evident and the elemental concentrations at the onset of the altered biotite layer are consistent across all sections and for each of the measured elements. The overall root mean square deviation (RMSD) between modelled and experimental data was calculated to be 0.11 (RMSD of 0 would be an ideal fit). The values of the fitting parameters (R_H, R_{Bti}, K_P, D_{ALT}, D_{Bt} and x_{bd}) used in the model and its output, t_r are listed in Table 2 and discussed in Section 5.2.

5. DISCUSSION

5.1. Mineral alteration underneath living hypha

Unlike many classical biotite dissolution studies, which typically quantified alteration at the macroscopic level from changes in solution chemistry, our perspective on biotite myco-weathering is based on nanometer to sub-micrometer scale analytical evidence of the interface between the fungi and the mineral substrate. Below, we develop consistent points of comparisons between our fungal and our abiotic dissolution datasets and various other literature datasets of abiotic and microbial biotite dissolution in order to determine the weathering efficiency of mycorrhiza.

Our data shows that, in addition to an increasing K mobilization with contact time, Fe, Al, Mg were also removed from the biotite substrate (Fig. 5) but with a delayed onset of mobilization of ~13 days (Fig. 6A and C, and Table 2). Interestingly, in all FIB sections, Si and O appeared preserved throughout the depth-profile (Fig. 2A), implying a non-stoichiometric dissolution and the formation of an Si/O-enriched "altered biotite" layer directly underneath the hypha. Overall, the mobilization of elements was visible up to ~40 nm deep into the mineral substrate (Figs. 2B, S4 and 5) including an "altered biotite" layer of up to ~20 nm. This "altered biotite" layer is marked by a different chemical (Figs. 2B and S7) and mineralogical composition compared to the bulk non-altered biotite (Bonneville et al., 2009). Furthermore, this "altered biotite" layer is crucial as it controls the elemental diffusion rate – and so the flux of elements towards the hypha – and also the migration of the moving boundary deeper into the biotite (Fig. 4).

The formal identification of the mineral phase that makes up this "altered biotite" layer is however difficult. The layer is extremely thin (~20 nm maximum) and even selected area electron diffraction (SAED) could not conclusively point to a change in diffraction pattern from the structure of the parent-mineral, biotite. Nevertheless, in our previous work (Bonneville et al., 2009), high-resolution TEM images revealed, within 30 nm of the interface with the hypha, (0 0 1) spacing domains of 14.0 Å as opposed to 10.0 Å for bulk non-altered biotite. These larger d-spacings are indicative of a transformation towards a vermiculite-type phase (Wierzchos and Ascaso, 1998). This is not surprising as vermiculite is the prime alteration product in acidic dissolution experiments of biotite containing more than ~0.8 Mg per $O_{10}(OH)_2$ (Murakami et al., 2003), a value which is close to the Mg content of our biotite (~0.77 Mg per $O_{10}(OH)_2$). Other secondary phases that may form during biotite alteration (e.g., Fe^{3+} (oxidized-) biotite) are more difficult to distinguish from pristine biotite based solely on high-resolution TEM micrographs because, depending on the extent of oxidation, their (0 0 1) d-spacing range from 10.1 to 10.3 Å (Jeong et al., 2006).

In this respect, the elemental removal from the "altered biotite" layer (Al, Fe, Mg and K depletions by ~75–85%, 80–85%, 55–75% and 50–65% compared to the bulk non-altered biotite; Fig. S7) further reinforces our previous evidence of a mineralogical transformation of biotite underneath the hypha. It is likely that the loss of the interlayer (K) and octahedral cations (Mg, Fe and Al) mobilized during fungal alteration are partially compensated by the Fe(II) oxidation into Fe(III). We have previously shown (Bonneville et al., 2009; Smits et al., 2009), that a ~200 nm layer of biotite directly underneath the hypha was enriched in Fe(III) compared to the bulk non-altered biotite. Considering the substantial removal of cations from the biotite, the positive charge loss is however unlikely to be balanced only by structural Fe(II) oxidation alone.

More likely, proton incorporation due to a pH shift at the surface of the biotite is occurring (Turpault and Trotignon, 1994). Incorporated protons, i.e., positive charges, are probably continuously "hopping" from one interstitial position to another to charge balance the removal of cations at depth in the mineral structure (Hawthorne, 1992). The micron-scale pH measurement in the current study using fluorescent probes confirmed that the hypha filaments growing in contact with the biotite acidified substantially their near-environment by, at least one pH unit (Fig. 3A and C). Acidification is a well-known fungal response characteristic due to the proton efflux resulting from the activity of the plasma-membrane H^+-ATPase and CO_2 production linked to the respiration of the hypha (Jones et al., 2004; Gadd, 2007) and to the exudation of organic acids (Rosling et al. (2004). Even though most of the fungal exudates are weak acids, it is possible that such organic acids may have contributed to the micron scale acidification. However, at high resolution we did not observe any precipitates of oxalate or any other for that matter (Bonneville et al., 2009), yet low levels of oxalic acid have been detected by infrared analyses of non-symbiotic

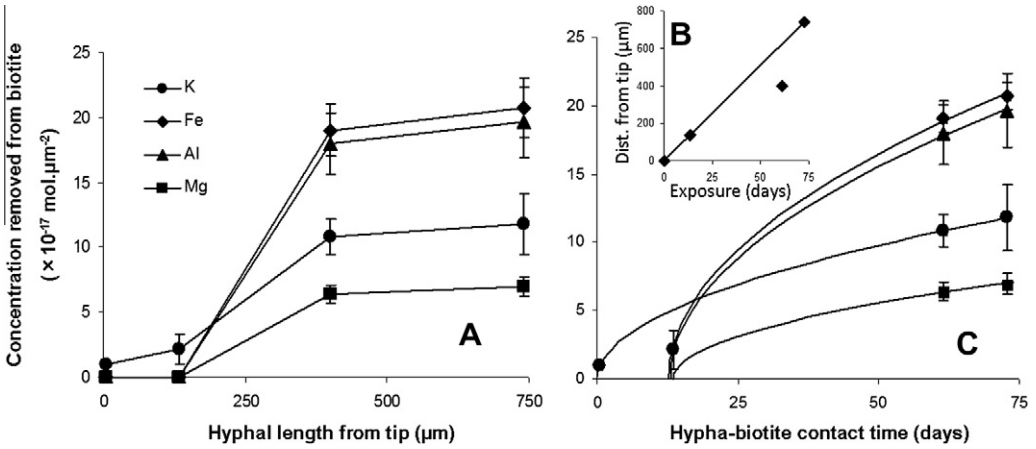

Fig. 6. (A) Longitudinal alteration profile, expressed as elemental concentration removed from the biotite along the sampled hypha. (B) Relationship between the distance of each FIB section from the hypha tip and the exposure time calculated from the alteration model. Line indicates the hyphal extension rate used in the alteration kinetics calculation (i.e., 10.2 µm day^{-1}). (C) Data (symbols) and modelled concentrations removed (solid lines) from the biotite as a function of the estimated contact time.

mycorrhiza grown over this same biotite (Schmalenberger et al., 2010).

In general, the alteration features and the mineralogical changes observed in the current study are in agreement with previous biotite dissolution studies. Incongruent biotite dissolution in acidic conditions has been reported in various experiments in batch, fluidized bed or flow-through systems (Acker and Bricker, 1992; Turpault and Trotignon, 1994; Kalinowski and Schweda, 1996; Malmstrom and Banwart, 1997). Turpault and Trotignon (1994) observed that a 200–400 nm altered layer enriched in Si and O formed from the (0 0 1) basal plane surface of biotite exposed to a pH ~1 solution. In the presence of bacteria, the dissolution of biotite was also shown to be incongruent and greatly enhanced with final Si, Fe and Al concentrations up to two orders of magnitude higher than in abiotic controls (Barker et al., 1998; Hopf et al., 2009). To the best of our knowledge, for fungi grown in non-aqueous media and in symbiosis with a tree, our results are the first to show: (a) an *in situ* elemental removal from a mineral substrate; (b) the formation of an altered biotite layer with a different chemical and mineralogical composition directly underneath a living hypha; and (c) a close spatial relationship between these alteration features and a fungal-driven acidification at the mineral surface. Combining all these observations and the mathematical framework described above allowed us to quantify element fluxes from a mineral substrate to a single living hypha.

5.2. Quantification of elemental fluxes at the hypha–biotite interface

To quantify the elemental fluxes and therefore the kinetics of fungal alteration, the exposure time between the biotite and the hypha needed to be determined. First, using the modelled curves in Fig. 5, the amounts of K, Mg, Fe and Al removed (in mol µm^{-2}) from the biotite were calculated for each of the four FIB sections (Table 3). Plotted against distance from the hypha tip, the elemental removal in each FIB section provides a longitudinal transect of alteration underneath the hypha (Fig. 6A). As the removal of potassium starts as soon as the hypha interacts with the biotite surface (Fig. 5), we could "time"-calibrate our model with the K depth-profiles. Using values for D_{Bt} from Taylor et al. (2000), we constrained D_{ALT} for K (see model description in Section 4 above) and thus derived the active period

Table 3
Calculated amounts of K, Al, Fe and Mg removed from biotite for each FIB section (standard deviations in brackets). The model data for the integrated amounts of elements mobilized along the entire length of the hypha and the associated elemental release and alteration rates are also listed.

Mycorrhizal alteration	K	Mg	Fe	Al
Section 1 (×10^{-17} mol element µm^{-2})	0.97 (0.16)	–	–	–
Section 2 (×10^{-17} mol element µm^{-2})	1.08 (0.12)	–	–	–
Section 3 (×10^{-17} mol element µm^{-2})	1.18 (0.14)	6.41 (0.68)	19.0 (1.90)	17.9 (2.34)
Section 4 (×10^{-17} mol element µm^{-2})	2.15 (0.24)	6.97 (0.75)	21.0 (2.16)	20.7 (2.71)
Total amount of elements removed from the biotite (×10^{-13} mol per hypha)	2.7	1.5	4.6	4.4
Release rate (×10^{-8} mol elements m^{-2} h^{-1})	4.5	2.4	7.2	6.8
Biotite alteration rate (×10^{-8} mol Bt m^{-2} h^{-1})	4.9	3.2	4.5	4.6

of alteration (t_r) for each of the four FIB sections: 0.4, 13.5, 61.4 and 72.8 days, respectively (Table 2).

Assuming constant and continual growth of the fungi over the biotite, a distance of 740 μm between FIB sections 1 and 4, yields an average hyphal growth rate of 10.2 μm d^{-1} (Fig. 6B). The actual hyphal growth mechanisms or rates over a biotite surface (or any other mineral surface for that matter) are unknown. The only values available for hyphal turnover rates in soils vary from 7 days (Staddon et al., 2003) to 145 days (Treseder et al., 2010). Thus, an independent check of our hyphal growth rate estimate is difficult. Nevertheless, considering the overall duration of the microcosm experiment (~130 days) and that the hypha had to grow first from the root to the biotite flake (Fig. 1A), a weathering active hypha–biotite interaction period of ~73 days for the FIB section 4 (Table 2) and thus the estimated hyphal growth rate (10.2 μm d^{-1}) seems reasonable. These values of hyphal growth rate and active-weathering periods were hereafter used to calculate the mycorrhizal alteration rates.

Time quantification for the Al, Fe and Mg profiles is more complex as their respective mobilization starts between FIB section 2 and FIB section 3. However, knowing: (i) the depth of the "altered biotite" layer (x_{bd}) from the Al, Fe and Mg profiles in FIB sections 3 and 4 (Figs. S4 and 5), (ii) the respective D_{Bt}/D_{AL} ratios (from the fits of the "diffusion front"), (iii) the amounts of each element removed (Table 3) in FIB sections 3 and 4 and (iv) the absolute exposure periods of FIB sections 3 and 4 (i.e., 61.4 and 72.8 days based on the above K profile analysis), allowed us to constrain the diffusion coefficient values for Al, Mg and Fe in the bulk non-altered biotite (D_{Bt}; Table 2). This then enabled the estimation, from the fitted model, of the concentration of elements removed (in mol μm^{-2}) from the biotite as a function of exposure time between the hypha and the biotite surface (Fig. 6C).

Similar to the classical dissolution scheme for biotite described by Malmstrom and Banwart (1997) and Schnoor (1990), in our experiments K was mobilized first, creating a K-depleted biotite layer, while Mg, Fe and Al only started to diffuse ~13 days after the initial hypha–biotite contact. The rate of K, Mg, Fe and Al removal from the biotite decreases sharply with contact time because the thickening of the "altered biotite" layer ultimately slows down the bulk biotite breakdown (Fig. 6C). The relatively low removal of K observed in FIB section 2 (Fig. 6C) compared to the modelled K curve indicates some degree of heterogeneity in the alteration process along the hypha possibly reflecting the hyphal pH variations (Fig. 3) and which is also in accordance with the formation of discrete vermiculite-like domains as-seen in high resolution TEM micrographs (Bonneville et al., 2009). Overall, our solid-state diffusion model captures the essential features of elemental removal within each FIB section but also provides a kinetic framework for myco-alteration along a living hypha attached to a mineral surface.

In order to derive the hyphal alteration rate, we also had to determine the contact surface area between hypha and biotite. Our FEG-SEM and Environmental SEM observations in Bonneville et al. (2009) showed that surface-bound hypha exhibited flattened shapes (although turgidity can be observed at the tip level) with an average width of ~5 μm. Combined with a total length of 740 μm, the sampled hypha had therefore a contact surface are with the biotite of ~3700 μm^2. It is to be noted however, that *P. involutus* hypha can form an ultrathin layer that may expand laterally. However so far there is no indication that this "biolayer" mediates alteration itself (Saccone et al., 2009). By integrating the curves in Fig. 6C and using the above hyphal contact surface area with biotite, the total removed K, Al, Mg and Fe from the biotite was estimated to be 2.7, 4.4, 1.5 and 4.6×10^{-13} mol, respectively. This corresponds to an elemental uptake/release of 4.5, 6.8, 2.4, 7.2×10^{-8} mol m^{-2} h^{-1} and thus a biotite hyphal alteration rate ranging from 3.2 to 4.9×10^{-8} mol of biotite m^{-2} h^{-1} (Table 3).

5.3. Biotite alteration kinetics: mycorrhizal *vs.* abiotic

Finally, in order to quantify the potential enhancing effect of mycorrhiza on the dissolution of biotite, both the fungal and the abiotic alteration kinetics need to be *consistently* compared. However, to carry out such a comparison several aspects have to be considered. Firstly, biotite dissolution rates are impacted by pH and to a lesser extent by temperature. Secondly, the experimental conditions for biotite weathering differ dramatically between experiments performed with mycorrhiza (either in liquid cultures, in pots or in microcosms) and most abiotic dissolution experiments (in solution, in batch or flow-through systems). For instance, in our microcosm experiments, the sampled hypha had grown over and interacted only with the basal plane (i.e., (001)) of the biotite flake. Conversely, in a typical abiotic experiment, the biotite particles are in constant and complete contact with the reacting solutions inducing a simultaneous dissolution of the edge and the basal plane. This is important, because biotite dissolution rates are highly, spatially anisotropic. The edge dissolution rate is between 36 and 240 times faster than basal plane dissolution rates (Turpault and Trotignon, 1994). Similar edge *vs.* basal plane differences in reactivity have been reported from Atomic Force Microscopic (AFM) measurements on biotite by (Aldushin et al., 2006) and phlogopite – a closely related phyllosilicate (Rufe and Hochella, 1999). Thus, in order to evaluate unambiguously the alteration "efficiency" of mycorrhiza, it is essential to assess the abiotic basal plane dissolution rate of the biotite used in our abiotic batch and flow through dissolution experiments. From the data from our abiotic experiments at pH 2, 3.3 and 4 (Fig. S5) the bulk dissolution rates (r_{bulk} in mol Bt m^{-2} h^{-1}), were calculated (Table 1). In addition, based on FEG-SEM image analyses, the ratios of basal ($SA_{basal}/SA_{total} \sim 0.94$) and edge ($SA_{edge}/SA_{total} \sim 0.06$) areas relative to the total geometrical surface area were determined. Thus, the biotite dissolution rates for the abiotic dissolution experiments can be defined as:

$$r_{bulk} = \frac{SA_{edge}}{SA_{total}} r_{edge} + \frac{SA_{basal}}{SA_{total}} r_{basal} \quad (13)$$

Where r_{edge} and r_{basal} were the specific dissolution rates of the edge and basal planes of our biotite (in mol Bt m^{-2} h^{-1}). Knowing that $36 < (r_{edge}/r_{basal}) < 240$ (Turpault and Trotignon, 1994), and having determined experimentally the values of r_{bulk} (Table 1), and having measured the relative proportions of basal and edge surface areas of our biotite from the FEG-SEM images, allows for Eq. (13) to be rearranged to obtain ranges for r_{basal} and r_{edge} for all our abiotic dissolution experiments (Table S1 in Supplementary information).

To compare our mycorrhizal and abiotic biotite dissolution data, a plot of dissolution rates *vs.* pH was constructed using the bulk dissolution rate data from the literature (open circles in Fig. 7) from which an average pH-dependency for the biotite dissolution kinetics was determined (Eq. (S1) and (S2) in Supplementary information). This was then applied to linearly extrapolate the range of r_{edge} and r_{basal} over the pH range between 1 and 6 (slanting gray areas bars in Fig. 7).

As expected, the calculated interval for the edge dissolution rates in our abiotic dissolution experiments is much faster than the bulk dissolution rate from literature (open circles) but in good agreement with the experimentally-defined edge dissolution rates data of (Bickmore, 2001) and (Balogh-Brunstad et al., 2008a) (i.e., open and half-filled triangles in Fig. 7). Conversely, the calculated interval for the basal plane dissolution rate is in the low-end of the bulk dissolution data from the literature. Only the bulk dissolution rate of (Taylor et al., 2000) – half filled circle in Fig. 7 – falls substantially lower than the calculated range for basal plane dissolution rates due to the use of larger particles compared to other studies and thus, a larger basal plane contribution.

In Section 5.2, the rate of dissolution of the biotite basal plane by mycorrhiza was estimated to be 3.2–4.9×10^{-8} mol of biotite m^{-2} h^{-1}. Yet, to consistently compare mycorrhizal and abiotic dissolution rates, the pH at which mycorrhiza altered the biotite substrate needs to be determined. This is problematic as hyphal pH varies greatly along the hypha length and this can reach more than one pH unit over 20 μm of hypha (for example see Fig. 3B) and these values can also potentially change with time. Minor pH variations along hypha lengths ($\Delta pH < 0.1$ pH units, the tip being slightly more alkaline than the rest of the hypha) have been previously reported by Schreurs and Harold (1988) and Limozin et al. (1997). The difference in pH variations along hypha between these studies and our observations is likely due to very different experimental conditions. In addition, in our experiments, hypha acidification was intense and substantial portions of analyzed hypha (~60 μm) exhibited pH values below our detection limit (i.e., pH 4.6; Fig. S1). Thus, the lowest pH could potentially have been even lower than pH 4.6 in some parts of the hypha. Although our confocal measurements are, so far, probably the most accurate estimates of pH of living hypha on mineral surface, further work is needed to fully quantify the pH of hypha especially in the acidic pH range and also to follow the evolution of hyphal pH over time. Despite the limitation of our pH-sensitive probe method, some conclusions can still be drawn with respect to the efficiency of hypha to alter biotite.

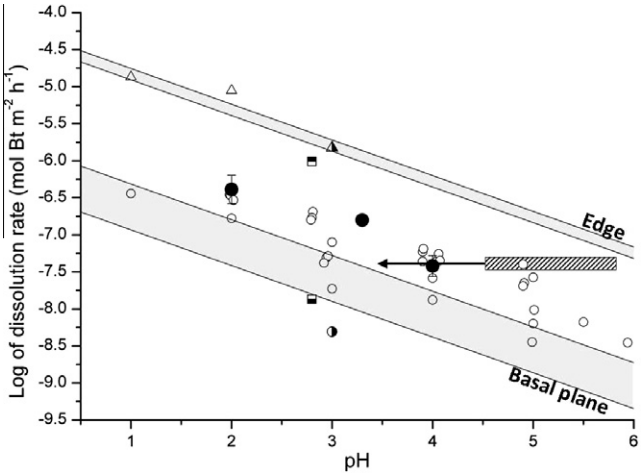

Fig. 7. Dissolution rates of biotite normalized to $-O_{10}(OH)_2$ as a function of pH. (○) denotes abiotic bulk dissolution rates from the literature (Acker and Bricker, 1992; Kalinowski and Schweda, 1996; Malmstrom and Banwart, 1997) and (◑) from (Taylor et al., 2000). (●) are the bulk batch abiotic control dissolution rates at pH 2 and 4 (this study) and at flow-through rates at pH 3.3 (this study). Triangles depict the edge dissolution rate: (◭) and (△) from Balogh-Brunstad et al. (2008a,b) and Bickmore (2001), respectively. Squares represent mycorrhizal dissolution rates: (⬒) and (⬓) illustrate the bulk and the basal plane dissolution rates respectively, from Balogh-Brunstad et al.'s (2008a,b) experiments with fungi liquid monocultures. Finally, the mycorrhizal basal plane alteration rate from the current study (◪) is plotted across a pH range measured (4.6–5.8) but with the arrow extending until pH 3.5 reflecting the lower pH boundary of acidic soils from the literature (Finkl, 2008). N. B. All abiotic (i.e., bulk, basal and edge) dissolution rates as well as those for the fungi monoculture in Balogh-Brunstad et al. (2008a,b) were performed at 25 °C as opposed to the 15 °C in the current microcosm experiment. All abiotic dissolution rates were therefore temperature corrected using the Arrhenius equation and a pH-dependant energy of activation ranging from 67 to 10 kJ mol^{-1} from pH 1 to pH 6 (Carroll and Walther, 1990).

To our knowledge, only Wallander et al. (1999) measured bulk soil pH during biotite alteration experiments with *P. involutus–P. sylvestris* symbiosis, in pot experiments. Their final bulk pH values varied between 4.8 and 5.2, in line with our biotite-bound hypha pH measurements. Except in soils subjected to pyrite oxidation, where pH can reach values as low as 2, acidic soils, such as podzols that are common in boreal forest, exhibits average bulk soil pH values between 3.5 and 5.5 (Finkl, 2008). Taking the latter pH of 3.5 as the low end of possible hyphal pH and pH 5.8 as the upper limit of surface-bound hypha (Fig. 3C), reveals that surface-bound hypha can substantially accelerate the dissolution of the basal plane (0 0 1) of biotite when compared to abiotic dissolution at equivalent pH conditions (gray hashed rectangular box and arrow in Fig. 7).

Quantifying this fungal alteration enhancement (i.e., beyond the hyphal acidification pH) is difficult as it obviously depends heavily on the local hyphal pH conditions: if hyphal pH is lower than the minimum of 3.5, both abiotic and mycorrhizal rates would be almost equivalent. However, in the case of hyphal pH values above 3.5, biotite alteration underneath surface-bound hypha is consistently faster than under abiotic conditions at equivalent pH. Here, we hypothesize that this 'extra' alteration capacity of surface-bound hypha is due to the ability of fungi to simultaneously disrupt mechanically the lattice structure of the mineral substrate on which it grows (Bonneville et al., 2009) and that, in turn, the weakened biotite zone directly underneath the hypha is more prone to chemical alteration.

In Fig. 7, we plotted also data from mycorrhizal monocultures in liquid media (half-filled squares) in the presence of biotite (Balogh-Brunstad et al., 2008a). These authors showed that basal plane alteration accounts for only 1% of the total alteration dissolution rate and concluded that "fungal weathering predominantly occurred not by attachment and direct transfer of nutrients via hyphae, but due to the exuded organic acids in the bulk liquid which accelerated dissolution of the flake edges". Our results from the plant-mycorrhiza-biotite continuum microcosms (unsaturated conditions) do not support this purely "exudate/liquid-only" alteration pathway. In addition to the fact that liquid mono-culture may lead to different fungal phenotypes than those observed in soils (Smith and Read, 2008), another aspect in the approach used by Balogh-Brunstad et al., (2008a,b) may further explain the difference between our respective findings. In Balogh-Brunstad et al. (2008a), the biotite basal plane dissolution rate was determined from volume-loss calculations due to fungal channelling based on Atomic Force Microscopic (AFM) observations after exposure of biotite with *Suillus tomentosus,* another common ectomycorrhiza strain, in liquid mono-culture. Thus, any fungal-induced element removal and thus chemical alteration at depth within the biotite basal plane, which we clearly showed in this study to be substantial, could not be considered as this removal occurs without volume-loss. Therefore, possibly, the mycorrhizal basal plane dissolution rate in Balogh-Brunstad et al. (2008a) was actually highly underestimated when compared to the present study. Nevertheless, fungal basal plane biotite dissolution is unlikely to be as fast as edge dissolution and, *under saturated hydric conditions and in a close system* (i.e., batch liquid mono-culture), the main biotite alteration is probably edge dissolution mediated by solution acidification essentially due to fungal respiration. However, when considering the occurrence of mycorrhiza fungi in natural soils, they are rarely found in saturated conditions. Many mycorrhizal species are highly hydrophobic and water-intolerant due to their aerobic respiration metabolic needs (Slankis, 1974). Indeed, mycorrhiza do not colonize tree roots in waterlogged soils (Theodorou, 1978) and, for instance, even very brief submersion (mins) are enough to inhibit the colonization of *P. sylvestris* roots by *Suillus* sp. (Strenström, 1991). Therefore, substantial fungal acidification of large volumes of water relative to the hypha dimensions, particularly on a relatively short timescale (before it percolates deeper, i.e., in an open system), is probably a rare occurrence in soils.

All these lines of evidence indicate that our study marks a step-change in the understanding of myco-weathering; surface-bound hypha can alter substantially the biotite basal plane, a surface often quoted as "inert" in terms of abiotic dissolution (Rufe and Hochella, 1999). Furthermore, we showed that surface-bound mycorrhiza can alter biotite in a humid environment, yet with no free water present. As such, these findings shift the way mineral weathering needs to be conceptualized and studied, with water not being the sole media controlling mineral alteration reactions.

6. CONCLUSIONS

In our experiments, the zone of contact between hypha and biotite is an alteration "hot-spot" where chemical weathering rates were greatly accelerated. This alteration enhancement is due to the synergy between (i) a biomechanical process during which the biotite lattice structure is disrupted as the hypha grow over the surface as shown in Bonneville et al. (2009) and (ii) a chemical alteration with hyphal μm-scale acidification, structural Fe(II) oxidation and cation removal at depth directly underneath the hypha. Here, we also showed that the elemental transfer from the biotite into the hyphae can be modelled as a solid-state diffusion process inducing the breakdown of biotite and the formation of an "altered biotite" layer. With time, the thickening "altered biotite" layer slows down/limits the overall mineral weathering rate and thus the release of nutrient from the mineral substrate. The declining nutrient flux may potentially trigger further growth of the hypha filament in order to renew/maintain the nutrient flux by interacting with a "fresh" non-altered mineral surface.

It is important to emphasize that this "interfacial" myco-alteration takes place on the basal plane of biotite, a low-reactivity mineral surface in terms of abiotic dissolution, yet representing the vast majority of the biotite surface typically exposed in soils (in itself ~7% of the total surface of exposed Earth's crust; Nesbitt and Young, 1984). In soils, mycorrhiza also acquire nutrients from organic matter or litter degradation. However, this recycling of nutrients cannot be perfect and, thus, the maintenance of vegetation requires prolonged and continual *de novo* rock decomposition. Mycorrhiza, because of their unique ability

to "sense" nutrient-rich substrates (Leake et al., 2008) and, as demonstrated here, to "boost" nutrition acquisition from raw rock-forming minerals, may therefore contribute largely to the long-term maintenance of vegetation.

Our approach has limitations. It is based on restricted number of observations along a single hypha grown in an experimental system that does not account for the whole complexity of soil biotia involved in the alteration process such as bacteria, metazoans or even earthworms (Suzuki et al., 2003) nor does it take into consideration the effect that these organisms can have on fungal alteration activity (Balogh-Brunstad et al., 2008b), viability or growth (Rainey, 1991). Our study represents an idealized system where fungi have no competitor and where the pine tree is fully dependent on mycorrhiza for nutrient acquisition. Therefore, our results, although the first of their kind, are, at beast, an upper estimate of the weathering capacity of single hypha in the field. Nevertheless, further work is needed to incorporate and to upscale alteration patterns observed at the hypha scale into a broader kinetic framework describing mycorrhizal weathering activity in soils (Brantley et al., 2011).

ACKNOWLEDGEMENTS

Funding from the UK Natural Environment Research Council "Weathering Science Consortium" NE/C004566/1 is acknowledged. The authors thank John Harrington and Rik Brydson and the Leeds Electron Microscopy and Spectroscopy Centre for help with the FIB sampling and discussions about STEM data interpretation. A. Duran, M. Smits and J. Leake from the Department of Animal and Plant Sciences and Maria Romero-Gonzalez and the Department of Civil and Structural Engineering at the U. of Sheffield are acknowledged for their help during the microcosm experiments. The authors acknowledge the travel grant from the UK Geological Society for A. Bray to travel to the Science Institute at the University of Iceland to carry out the abiotic flow-through experiments under the supervision of Dominik Wolff-Boenisch. Linda Forbes and Eric Condliffe, University of Leeds are thanked for her help with ICP-MS and EMPA analyses respectively. M. Krom and C. Peacock are thanked for reviewing the manuscript. The authors also thank the three anonymous reviewers and the associate editor C. Daughney for helpful comments during the review process.

APPENDIX A. SUPPLEMENTARY DATA

Supplementary data associated with this article can be found, in the online version, at doi:10.1016/j.gca.2011.08.041.

REFERENCES

Acker J. G. and Bricker O. P. (1992) The influence of pH on biotite dissolution and alteration kinetics at low temperature. *Geochim. Cosmochim. Acta* **56**, 3073–3092.

Adeyemi A. O. and Gadd G. M. (2005) Fungal degradation of calcium-, lead- and silicon-bearing minerals. *Biometals* **18**, 269–281.

Aldushin K., Jordan G. and Schmahl W. W. (2006) Basal plane reactivity of phyllosilicates studied in situ by hydrothermal atomic force microscopy (HAFM). *Geochim. Cosmochim. Acta* **70**, 4380–4391.

Amalfitano S. and Fazi S. (2008) Recovery and quantification of bacterial cells associated with streambed sediments. *J. Microbiol. Meth.* **75**, 237–243.

Balogh-Brunstad Z., Keller C. K., Dickinson J. T., Stevens F., Li C. Y. and Bormann B. T. (2008a) Biotite weathering and nutrient uptake by ectomycorrhizal fungus, *Suillus tomentosus*, in liquid-culture experiments. *Geochim. Cosmochim. Acta* **72**, 2601–2618.

Balogh-Brunstad Z., Keller C. K., Gill R. A., Bormann B. T. and Li C. Y. (2008b) The effect of bacteria and fungi on chemical weathering and chemical denudation in pine growth experiments. *Biogeochemistry* **88**, 153–167.

Barker W. W., Welch S. A., Chu S. and Banfield J. F. (1998) Experimental observations of the effects of bacteria on aluminosilicate weathering. *Am. Mineral.* **83**, 1551–1563.

Bennett H. E., Peck R. L., Burge D. K. and Bennett J. M. (1969) Formation and growth of tarnish on evaporated silver films. *J. Appl. Phys.* **40**, 3351–3361.

Berner R. A. (1992) Weathering, plants, and the long-term carbon cycle. *Geochim. Cosmochim. Acta* **56**, 3225–3231.

Berner R. A. (1995) Chemical weathering and its effect on atmospheric CO_2 and climate. *Rev. Mineral.* **31**, 565–583.

Berner R. A. (2003) The long-term carbon cycle, fossil fuels and atmospheric composition. *Nature* **426**, 323–326.

Berner R. A. and Kothavala Z. (2001) Geocarb III: a revised model of atmospheric CO_2 over Phanerozoic time. *Am. J. Sci.* **301**, 182–204.

Bickmore B. R. (2001) Edge surface area normalized dissolution rates of biotite and montmorillonite. In *Atomic Microscopy Study of Clay Mineral Dissolution*. Ph. D. Dissertation, Virginia Polytechnic Institute and State University, pp. 49–76.

Bonfante P. (2003) Plants, mycorrhizal fungi and endobacteria: a dialog among cells and genomes. *Biol. Bull.* **204**, 215–220.

Bonneville S., Behrends T., Van Cappellen P., Hyacinthe C. and Roling W. F. M. (2006) Reduction of Fe(III) colloids by *Shewanella putrefaciens*: a kinetic model. *Geochim. Cosmochim. Acta* **70**, 5842–5854.

Bonneville S., Smits M. M., Brown A., Harrington J., Leake J. R., Brydson R. and Benning L. G. (2009) Plant-driven fungal weathering: early stages of mineral alteration at the nanometer scale. *Geology* **37**, 615–618.

Brantley S. L., Megonigal J. P., Scatena F. N., Balogh-Brunstad Z., Barnes R. T., Bruns M. A., Van Cappellen P., Dontsova K., Hartnett H. E., Hartshorn A. S., Heimsath A., Herndon E., Jin L., Keller C. K., Leake J. R., McDowell W. H., Meinzer F. C., Mozdzer T. J., Petsch S., Pett-Ridge J., Pregitzer K. S., Raymond P. A., Riebe C. S., Shumaker K., Sutton-Grier A., Walter R. and Yoo K. (2011) Twelve testable hypotheses on the geobiology of weathering. *Geobiology* **9**, 140–165.

Buss H. L., Luttge A. and Brantley S. L. (2007) Etch pit formation on iron silicate surfaces during siderophore-promoted dissolution. *Chem. Geol.* **240**, 326–342.

Carroll S. A. and Walther J. V. (1990) Kaolinite dissolution at 25 degrees, 60 degrees, and 80 degrees C. *Am. J. Sci.* **290**, 797–810.

Crane P. R., Friis E. M. and Pedersen K. R. (1995) The origin and early diversification of angiosperms. *Nature* **374**, 27–33.

Crank J. (1987) *Free and Moving Boundary Problems*. Oxford University Press, Oxford.

Derry L. A. (2006) Fungi, weathering, and the emergence of animals. *Science* **311**, 1386–1387.

Ehrlich H. L. (1998) Geomicrobiology: its significance for geology. *Earth Sci. Rev.* **45**, 45–60.

Ek H. (1997) The influence of nitrogen fertilization on the carbon economy of *Paxillus involutus* in ectomycorrhizal association with *Betula pendula*. *New Phytol.* **135**, 133–142.

Fishman M. J. and Friedman L. C. (1989) Methods for the determination of inorganic substances in water and fluvial sediments. *Techniques of Water-Resources Investigations of the United States Geological Survey,* Book 5, Chapter A1, USGS, Alexandria, VA.

Finkl C. W. (2008) Soils of the coastal zone. In *Encyclopedia of Soil Sciences* (ed. W. Chesworth). Springer, Dordrecht, pp. 711–733.

Gadd G. M. (2007) Geomycology: biogeochemical transformations of rocks, minerals, metals and radionuclides by fungi, bioweathering and bioremediation. *Mycol. Res.* **111**, 3–49.

Godderis Y., Roelandt C., Schott J., Pierret M.-C. and Francois L. M. (2009) Towards an integrated model of weathering, climate, and biospheric processes. *Thermodyn. Kinet. Water–Rock Interact. Rev. Mineral. Geochem.* **70**, 411–434.

Hawthorne F. C. (1992) The role of OH and H_2O in oxide and oxysalts minerals. *Z. Kristallogr.* **210**, 183–206.

Hobbie E. A. and Wallander H. (2006) Integrating ectomycorrhizal fungi into quantitative frameworks of forest carbon and nitrogen cycling. In *Fungi in Biogeochemical Cycles* (ed. G. M. Gadd). Cambridge University Press, Cambridge, pp. 98–128.

Hogsberg M. N. and Hogsberg P. (2002) Extramatrical ectomycorrhizal mycelium contributes one-third of microbial biomass and produces, together with associated roots, half the dissolved organic carbon in a forest soil. *New Phytol.* **154**, 791–795.

Hopf J., Langenhorst F., Pollok K., Merten D. and Kothe E. (2009) Influence of microorganisms on biotite dissolution: an experimental approach. *Chem. Erde-Geochem.* **69**, 45–56.

Hunter R. C. and Beveridge T. J. (2005) Application of a pH-Sensitive fluoroprobe (C-SNARF-4) for pH microenvironment analysis in *Pseudomonas aeruginosa* biofilms. *Appl. Environ. Microbiol.* **71**, 2501–2510.

Jastrow J. D., Miller R. M. and Lussenhop J. (1998) Contributions of interacting biological mechanisms to soil aggregate stabilization in restored prairie. *Soil Biol. Biochem.* **30**, 905–916.

Jeong G. Y., Cheong C.-S. and Kim J. (2006) Rb–Sr and K–Ar systems of biotite in surface environments regulated by weathering processes with implications for isotopic dating and hydrological cycles of Sr isotopes. *Geochim. Cosmochim. Acta* **70**, 4734–4749.

Jones D. L., Hodge A. and Kuzyakov Y. (2004) Plant and mycorrhizal regulation of rhizodeposition. *New Phytol.* **163**, 459–480.

Jongmans A. G., van Breemen N., Lundstrom U., van Hees P. A. W., Finlay R. D., Srinivasan M., Unestam T., Giesler R., Melkerud P. A. and Olsson M. (1997) Rock-eating fungi. *Nature* **389**, 682–683.

Kalinowski B. E. and Schweda P. (1996) Kinetics of muscovite, phlogopite, and biotite dissolution and alteration at pH 1–4, room temperature. *Geochim. Cosmochim. Acta* **60**, 367–385.

Kendrick P. and Crane P. R. (1997) The origin and early evolution of plants on land. *Nature* **33**, 39.

Kennedy M., Droser M., Mayer L. M., Pevear D. and Mrofka D. (2006) Late precambrian oxygenation: inception of the clay mineral factory. *Science* **311**, 1446–1449.

Kent D. A. and Triplett E. W. (2002) Microbial communities and their interactions in soil and rhizophere ecosystems. *Ann. Rev. Microbiol.* **56**, 211–236.

Landeweert R., Hoffland E., Finlay R. D., Kuyper T. W. and van Breemen N. (2001) Linking plants to rocks: ectomycorrhizal fungi mobilize nutrients from minerals. *Trends Ecol. Evol.* **16**, 248–254.

Leake J. R., Duran A. L., Hardy K. E., Johnson I., Beerling D. J., Banwart S. A. and Smits M. M. (2008) Biological weathering in soil: the role of symbiotic root-associated fungi biosensing minerals and directing photosynthate-energy into grain-scale mineral weathering. *Mineral. Mag.* **72**, 85–89.

Leyval C. and Berthelin J. (1991) Weathering of a mica by roots and rhizospheric microorganisms of pine. *SSSA J.* **55**, 1009–1016.

Leyval C., Surtiningish T. and Berthelin J. (1993) Mobilization of P and Cd from rock phosphates by rhizosphere microorganisms (phosphate dissolving bacteria and ectomycorrhizal fungi). *Phosphor. Sulphur Silicon* **77**, 133–136.

Lian B., Wang B., Pan M., Liu C. and Teng H. H. (2007) Microbial release of potassium from K-bearing minerals by thermophilic fungus *Aspergillus fumigatus*. *Geochim. Cosmochim. Acta* **72**, 87–98.

Limozin L., Denet B. and Pelce P. (1997) Ionic currents generated by tip growing cells. *Phys. Rev. Lett.* **78**, 4881–4884.

Malmstrom M. and Banwart S. (1997) Biotite dissolution at 25 °C: the pH dependence of dissolution rate and stoichiometry. *Geochim. Cosmochim. Acta* **61**, 2779–2799.

Marcotte N. and Brouwer A. M. (2005) Carboxy SNARF-4F as a fluorescent pH probe for ensemble and fluorescence correlation spectroscopies. *J. Phys. Chem. B* **109**, 11819–11828.

Mikutta R., Schaumann G., Gildemeister D., Bonneville S., Kramer M. G., Chorover J., Chadwick O. A. and Guggenberger G. (2009) Biogeochemistry of mineral–organic associations across a long-term mineralogical soil gradient (0.3–4100 kyr), Hawaiian Islands. *Geochim. Cosmochim. Acta* **73**, 2034–2060.

Mojallali H. and Weed S. B. (1978) Weathering of micas by mycorrhizal soybean plants. *SSSA J.* **42**, 367–372.

Moulton K. L., West J. and Berner R. A. (2000) Solute flux and mineral mass balance approaches to the quantification of plant effects on silicate weathering. *Am. J. Sci.* **300**, 539–570.

Murakami T., Utsunomiya S., Yokoyama T. and Kasama T. (2003) Biotite dissolution processes and mechanisms in the laboratory and in nature: early stage weathering environment and vermiculitization. *Am. Mineral.* **88**, 377–386.

Nesbitt H. W. and Young G. M. (1984) Prediction of some weathering trends of plutonic and volcanic rocks based on thermodynamic and kinetic considerations. *Geochim. Cosmochim. Acta* **48**, 1523–1534.

Paris F., Bonnaud P., Ranger J. and Lapeyrie F. (1995) In vitro weathering of phlogopite by ectomycorrhizal fungi. 1. Effect of K^+ and Mg^{2+} deficiency on phyllosilicate evolution. *Plant Soil* **177**, 191–201.

Pote J., Bravo A. G., Mavingui P., Ariztegui D. and Wildi W. (2010) Evaluation of quantitative recovery of bacterial cells and DNA from different lake sediments by Nycodenz density gradient centrifugation. *Ecol. Indicator* **10**, 234–240.

Rainey P. B. (1991) Effect of *Pseudomonas putida* on hyphal growth *Agaricus bisporus*. *Mycol. Res.* **95**, 699–704.

Rosling A., Lindahl B. D., Taylor A. F. S. and Finlay R. D. (2004) Mycelial growth and substrate acidification of ectomycorrhizal fungi in response to different minerals. *FEMS Microbiol. Ecol.* **47**, 31–37.

Rufe E. and Hochella M. F. (1999) Quantitative assessment of reactive surface area of phlogopite during acid dissolution. *Science* **285**, 874–876.

Saccone L., Gazze S. A., Ragnarsdottir K. V., Leake J. R., Duran A. L., Hallam K. R. and Mcmaster T. J. (2009) *Paxillus involutus* hyphae: imaging their structure and interaction with mineral surfaces using AFM. *Geochim. Cosmochim. Acta* **73**, A1140.

Schreurs W. J. A. and Harold F. M. (1988) Transcellular proton current in *Achlya bisexualis* hyphae: relationship to polarized growth. *Proc. Natl. Acad. Sci.* **85**, 1534–1538.

Schnoor J. L. (1990) Kinetics of chemical weathering: a comparison of laboratory and field weathering rates. In *Aquatic Chemical Kinetics* (ed. W. Stumm). Wiley, New York, YK.

Schmalenberger A., Duran A. L., Romero-Gonzales M. E., Leake J. R. and Banwart S. A. (2010) Oxalic acid release in ectomycorrhiza mineral weathering. *Geochim. Cosmochim. Acta* **74**, A923.

Slankis V. (1974) Soil factors influencing formation of mycorrhizae. *Annu. Rev. Phytopathol.* **12**, 437–457.

Smith S. E. and Read D. J. (2008) *Mycorrhizal Symbiosis*, third ed. Academic Press, San Diego.

Smits M. M., Bonneville S., Haward S. and Leake J. R. (2008) Ectomycorrhizal weathering, a matter of scale? *Mineral. Mag.* **72**, 131–134.

Smits M. M., Herrmann A. M., Duane M., Duckworth O. W., Bonneville S., Benning L. G. and Lundström U. (2009) The fungal–mineral interface: challenges and considerations of micro-analytical developments. *Fungal Biol. Rev.* **23**, 122–131.

Staddon P. L., Bronk Ramsey C., Ostle N., Ineson P. and Fitter A. H. (2003) Rapid turnover of hyphae of mycorrhizal fungi determined by AMS microanalysis of ^{14}C. *Science* **300**, 1138–1140.

Strenström E. (1991) The effects of flooding on the formation of ectomycorrhizae in *Pinus sylvestris* seedlings. *Plant Soil* **81**, 247–250.

Suzuki Y., Matsubara T. and Hoshino M. (2003) Breakdown of minerals grains by earthworms and beetle larvae. *Geoderma* **112**, 131–142.

Taylor A. S., Blum J. D., Lasaga A. C. and MacInnis I. N. (2000) Kinetics of dissolution and Sr release during biotite and phlogopite weathering. *Geochim. Cosmochim. Acta* **64**, 1191–1208.

Theodorou C. (1978) Soil moisture and the mycorrhizai association of *Pinus radiata* P. Don. *Soil Biol. Biochem.* **10**, 33–37.

Tobler D., Stefansson A. and Benning L. G. (2008) In-situ grown silica sinters in Icelandic geothermal areas. *Geobiology* **6**, 481–502.

Treseder K. K., Schimel J. P., Garcia M. O. and Whiteside M. D. (2010) Slow turnover and production of fungal hyphae during a Californian dry season. *Soil Biol. Biochem.* **42**, 1657–1660.

Turpault M.-P. and Trotignon L. (1994) The dissolution of biotite single crystals in dilute HNO_3 at 24 °C: evidence of an anisotropic corrosion process of micas in acidic solutions. *Geochim. Cosmochim. Acta* **58**, 2761–2775.

Wolff-Boenisch D., Gislason S. R. and Oelkers E. H. (2004) The effect of fluoride on the dissolution rates of natural glasses at pH 4 and 25 degrees C. *Geochim. Cosmochim. Acta.* **68**, 4571–4582.

Wallander H. and Wickman T. (1999) Biotite and microline as potassium sources in ectomycorrhizal and non-microrrhizal Pinus sylvestris seedlings. *Mycorrhiza* **9**, 25–32.

Wallander H. (2000) Uptake of P from apatite by *Pinus sylvestris* seedlings colonized by different ectomycorrhizal fungi. *Plant Soil* **218**, 249–256.

Wang B. and Qiu Y.-L. (2006) Phylogenetic distribution and evolution of mycorrhiza in land plants. *Mycorrhiza* **16**, 299–363.

Whitfield J. (2007) Fungal roles in soil ecology: underground networking. *Nature* **449**, 136–138.

Wierzchos J. and Ascaso C. (1998) Mineralogical transformation of bioweathered granitic biotite, studied by HRTEM: evidence for a new pathway in lichen activity. *Clay Clays Min.* **46**, 446–452.

Young I. M. and Crawford J. W. (2004) Interactions and self-organization in the soil–microbe complex. *Science* **304**, 1634–1637.

Associate editor: Christopher John Daughney